

Brain Tissue Segmentation Across the Human Lifespan via Supervised Contrastive Learning

Xiaoyang Chen, Jinjian Wu, Wenjiao Lyu, Yicheng Zou, Kim-Han Thung,
Siyuan Liu, Ye Wu, Sahar Ahmad, and Pew-Thian Yap^(✉)

Department of Radiology and Biomedical Research Imaging Center (BRIC),
University of North Carolina, Chapel Hill, NC, USA
[✉] ptyap@med.unc.edu

Abstract. Automatic segmentation of brain MR images into white matter (WM), gray matter (GM), and cerebrospinal fluid (CSF) is critical for tissue volumetric analysis and cortical surface reconstruction. Due to dramatic structural and appearance changes associated with developmental and aging processes, existing brain tissue segmentation methods are only viable for specific age groups. Consequently, methods developed for one age group may fail for another. In this paper, we make the first attempt to segment brain tissues across the entire human lifespan (0 – 100 years of age) using a unified deep learning model. To overcome the challenges related to structural variability underpinned by biological processes, intensity inhomogeneity, motion artifacts, scanner-induced differences, and acquisition protocols, we propose to use contrastive learning to improve the quality of feature representations in a latent space for effective lifespan tissue segmentation. We compared our approach with commonly used segmentation methods on a large-scale dataset of 2,464 MR images. Experimental results show that our model accurately segments brain tissues across the lifespan and outperforms existing methods.

1 Introduction

Segmentation of gray matter (GM), white matter (WM), and cerebrospinal fluid (CSF) from magnetic resonance (MR) images is a prerequisite for delineating brain anatomical structures and for quantifying changes in tissue volumes and cortical geometry in relation to development and aging. Manual brain tissue segmentation carried out by experts can be time-consuming, laborious, and sensitive to intra- and inter-rater variability. Therefore, effective automated segmentation approaches for brain tissues are highly desirable.

Although commonly employed segmentation methods, including SPM [1], FreeSurfer [3], and FSL [14] are effective in delineating brain tissues, they are tailored for adult MR images. These methods are less effective in segmenting infant brain MR images due to dynamic morphological and appearance changes caused by developmental processes during the first few years after birth. To cater to the unique characteristics of infant brains, the developing human connectome project (dHCP) processing pipeline [7] and Infant FreeSurfer [15] have

been developed. These are atlas-based segmentation methods, which warp manually segmented atlas to the target image using non-rigid registration methods. However, accurate segmentation of fine structures remains difficult due to large anatomical variability, leading to sub-optimal results. Inaccurate segmentation can cause problems in the reconstruction of the cortical surfaces need to measuring cortical morphology such as cortical thickness, surface area, and curvature.

Deep neural networks (DNNs) have been successfully used for brain tissue segmentation. For example, Roy et al. [10] first pretrained a model with auxiliary labels for a large unlabeled dataset using FreeSurfer and then fine-tuned the model with limited manually labeled data. Like FreeSurfer, this method is effective only for adult images. Nie et al. [9] trained multiple models, each of which is designed for a different imaging modality to segment images particularly in isointense phase ($\approx 6 - 8$ months of age). These methods are tailored for specific age groups and are not generalizable to other age groups.

In this paper, we propose a novel brain tissues segmentation method that is applicable across the entire human lifespan (0 – 100 years of age). Designing a unified model that takes into account the developmental and aging related structural and contrast changes in brain MR images (Fig. 1) is challenging. Moreover, common imaging issues such as noise, intensity inhomogeneity, partial volume effects, artifacts, and acquisition protocols further complicate model design. To address these problems, we propose to use supervised contrastive learning to learn discriminative feature representations that are robust to intensity differences and imaging imperfections.

The key contributions of our work are as follows: (i) We propose an unprecedented lifespan segmentation method based on a single deep learning model; (ii) We use novel supervised contrastive learning strategy to regularize network training to learn discriminative features that are robust to structural and tissue contrast changes driven by biological mechanisms, inconsistent acquisition protocols, and imaging imperfections; and (iii) We demonstrate on a large dataset of 2,464 brain MR images the effectiveness of our method.

2 Methods

2.1 Supervised Contrastive Learning

Despite architecture differences, deep learning segmentation models share two main components: (i) feature extractor (FE) and (ii) classifier. For medical image segmentation, the FE usually has an encoder-decoder architecture to enable full-resolution segmentation. The FE is used to learn voxel-wise feature representations. A classifier, which is usually implemented with one or a few $1 \times 1 \times 1$ convolutional layers, is used to perform voxel-wise classification by taking the feature representations learned by the FE as the input. Previous approaches typically jointly learn the FE and the classifier via a voxel-wise loss function such as categorical cross-entropy.

However, the above joint learning scheme is unable to learn discriminative features [13]. As a result, the margin between feature clusters with different

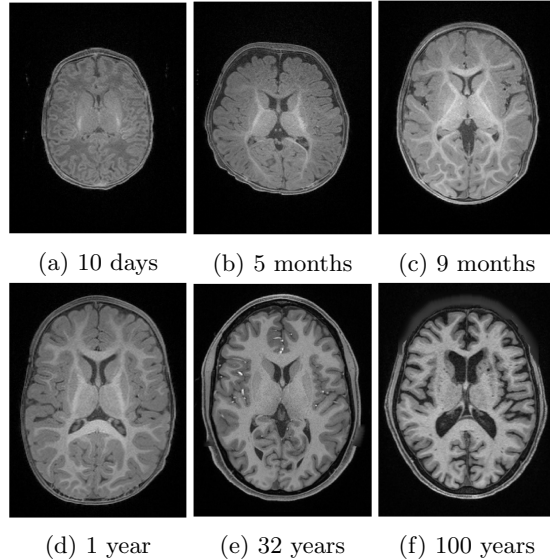


Fig. 1: Brain morphology and tissue contrast vary across the human lifespan.

labels is narrow, leading to error-prone classifiers and models that are sensitive to noise, artifacts, and intensity and contrast changes. Inspired by the success of Momentum Contrast (MoCo) [5], which is a self-supervised learning approach for instance discrimination, we adopt a similar contrastive learning strategy to learn discriminative features. Unlike MoCo, where contrastive learning is used for unsupervised pre-training, we perform contrastive learning in a supervised manner.

The key idea of contrastive learning is to pull the feature representations of the same class close together and push those from different classes far apart in a latent space. To this end, we use a memory bank to store a few typical feature representations as proxies for each semantic category. It should be noted that using proxies is more feasible than making pair-wise comparisons because around a million of voxels are involved at each training step in our case; otherwise, the problem becomes intractable. To implement contrastive learning, cosine similarity between a feature representation and the proxies in the memory bank is computed. Then, contrastive loss (i.e., InfoNCE) is calculated voxel-wise. We use the label of a given voxel as guidance to select positive and negative proxies from the memory bank and therefore we call our training strategy *supervised contrastive learning*.

We use a memory bank with the shape of $C \times M \times D$, where C is the number of semantic categories, M is number of proxies for each category, and D is the dimensionality of proxies. Note that D is identical to the number of channels of the last layer of the FE. The memory bank is trainable, adaptively learned and optimized via back-propagation during training. A proxy in the memory bank

acts as a positive proxy if a query (i.e., the feature representation of a voxel) shares the same label with it, otherwise it will be used as a negative proxy in calculating the contrastive loss.

The contrastive loss for an arbitrary query \mathbf{q}_i is defined as:

$$\mathcal{L}_{\text{ctr}}^i = -\frac{1}{M} \sum_{\{\mathbf{k}_i^+\}} \log \frac{\text{sim}(\mathbf{q}_i, \mathbf{k}_i^+)/\tau}{\text{sim}(\mathbf{q}_i, \mathbf{k}_i^+)/\tau + \sum_{\{\mathbf{k}_i^-\}} \text{sim}(\mathbf{q}_i, \mathbf{k}_i^-)/\tau}, \quad (1)$$

where $\text{sim}(\mathbf{u}, \mathbf{v}) = \frac{\mathbf{u}^\top \mathbf{v}}{\|\mathbf{u}\| \|\mathbf{v}\|}$ is cosine similarity, τ is the temperature hyper-parameter, \mathbf{q}_i is the feature representation of a query voxel with index i , $\{\mathbf{k}_i^+\}$ and $\{\mathbf{k}_i^-\}$ are the set of positive and negative proxies for \mathbf{q}_i , respectively. The size of sets $\{\mathbf{k}_i^+\}$ and $\{\mathbf{k}_i^-\}$ is equal to M and $M(C-1)$, respectively.

2.2 Joint Feature Regularization and Classification

In addition to $\mathcal{L}_{\text{ctr}}^i$ for feature regularization, categorical cross-entropy loss $\mathcal{L}_{\text{ce}}^i$ is used for joint training. The overall loss function $\mathcal{L}_{\text{total}}^i$ for query voxel i is a weighted sum of $\mathcal{L}_{\text{ce}}^i$ and $\mathcal{L}_{\text{ctr}}^i$, balanced by λ_{ctr} , and is formally defined as

$$\mathcal{L}_{\text{total}}^i = \mathcal{L}_{\text{ce}}^i + \lambda_{\text{ctr}} \mathcal{L}_{\text{ctr}}^i, \quad (2)$$

where

$$\mathcal{L}_{\text{ce}}^i = - \sum_{c=1}^C y_{ic} \log(\hat{p}_{ic}). \quad (3)$$

In (3), \hat{p}_{ic} is the c -th element of the output probability vector for query voxel i . y_{ic} , taking either 0 or 1, is the ground truth value for \hat{p}_{ic} .

2.3 Learning from Imbalanced Data

The class imbalance issue is common in brain tissue segmentation. At the image level, volumes of GM and WM are usually 2–3 times larger than that of CSF and all the three tissues are considerably smaller than the background region, i.e., the region that is not GM, WM or CSF. At the mini-batch level, the class imbalance issue can be even more severe, since an image patch is expected to contain only voxels from as few as one class.

We solve the class imbalance issue using two different approaches. The first approach is to use stratified sampling. Instead of randomly taking samples from the whole image region, we first derive the minimum bounding box of each tissue type using the ground truth label map and then randomly take an equal number of samples (i.e., image patches) from each tissue-specific bounding box. For simplicity, we allow overlapped bounding boxes. The second approach is to select an equal number of samples from each class that is present in a mini-batch for loss computation.

Due to randomness in sampling, the label set \mathbb{L} for a given mini-batch is only a subset of $\{0, 1, \dots, C-1\}$ (positive integers represent foreground class labels and

0 denotes the background). We first count the number of voxels for each category in \mathbb{L} and obtain the minimum $N_{\min} = \min\{N_c : c \in \mathbb{L}\}$, where N_c is the number of samples of class c in the mini-batch. We then randomly select N_{\min} samples from each category present in the mini-batch and compute the loss for each sample. The final loss is the average of the losses for the selected samples.

2.4 Implementation Details

We implemented the proposed method in Keras with TensorFlow as backend. We used a V-Net variant as the feature extractor. In contrast to the original V-Net [8], we (i) removed the original head for classification; (ii) adjusted the size of the convolutional kernel from 5 to 3 to lower the risk of overfitting; and (iii) used instance normalization [11] after each convolutional layer as it is suitable for small batch sizes. We used a simple multi-layer perceptron (MLP), consisting of three $1 \times 1 \times 1$ convolutional layers, as the classifier. In the MLP, the first two convolutional layers are followed by a rectified linear unit (ReLU) and the last one is followed by a softmax layer. We used the Adam optimizer with an initial learning rate of 0.0001 to update the parameters. The convolutional kernels and the memory bank were randomly initialized. The bias terms were initialized to 0. The patch size was set to $80 \times 80 \times 80$ and the batch size to 2.

3 Experimental Results

3.1 Dataset

The dataset consists of T1- and T2-weighted image pairs from five Lifespan Human Connectome Projects [12,4,15]: (i) Developing Human Connectome Project (dHCP; gestational age: 37 – 44 weeks) [7]; (ii) Baby Connectome Project (BCP, ages: 0 – 5 years) [6]; (iii) HCP Development (HCP-D, ages: 6 – 22 years); (iv) HCP Young Adult (HCP-YA, ages: 22 – 37 years); and (v) HCP Aging (HCP-A, ages: 36 – 100 years). Of the total 2,462 image pairs used, 682 were used for training, 113 for validation and the rest for testing. Among the images used for training, we manually annotated 62 images (high-quality set) and the tissue segmentation maps for the remaining 620 images (uncorrected set) were obtained using the standard HCP minimal preprocessed pipeline. The high-quality set includes 31 images from BCP, 20 from HCP-D, 7 from HCP-YA, and 4 from HCP-D. Since the number of images in the high-quality set is much smaller than in the uncorrected set, we take half of the training samples from the high-quality set and the other half from the uncorrected set to make sure the model is not biased to uncorrected labels. For testing, we used dice similarity coefficient (DSC) and average surface distance (ASD) as metrics for performance evaluation.

3.2 Experimental Setup

We compared the proposed method with the vanilla V-Net [8] and the V-Net variant (with the same MLP as the classification head). The V-Net variant and

Table 1: Comparison of DSC and ASD on the testing set for various methods.

Method	DSC (%)			ASD (mm)		
	GM	WM	CSF	GM	WM	CSF
V-Net [8]	81.4 ± 10.8	85.5 ± 7.6	77.3 ± 6.7	0.26 ± 0.11	0.45 ± 0.23	0.28 ± 0.13
V-Net variant	93.2 ± 1.6	95.4 ± 1.2	80.1 ± 6.2	0.08 ± 0.02	0.07 ± 0.02	0.22 ± 0.12
Proposed	94.2 ± 1.1	95.7 ± 1.0	88.5 ± 3.8	0.06 ± 0.01	0.07 ± 0.02	0.15 ± 0.07

Table 2: Comparison of DSC and ASD on the testing set with different inputs.

Modality	DSC (%)			ASD (mm)		
	GM	WM	CSF	GM	WM	CSF
T1	92.7 ± 3.0	95.1 ± 2.1	87.2 ± 6.5	0.09 ± 0.05	0.09 ± 0.06	0.17 ± 0.09
T2	92.3 ± 1.9	94.7 ± 1.8	88.1 ± 4.5	0.09 ± 0.02	0.09 ± 0.03	0.15 ± 0.06

the proposed method differ in that the V-Net variant was trained with categorical cross-entropy (CE) loss only.

3.3 Results

Main results The experimental results are shown in Table 1. The vanilla V-Net only achieves DSC of 81.4 ± 10.8 , 85.5 ± 7.6 and 77.3 ± 6.7 on GM, WM and CSF, respectively. Compared with vanilla V-Net, the V-Net variant significantly improves the performance by 11.8%, 9.9% and 2.8% on GM, WM and CSF, respectively ($p < 0.001$). With the proposed supervised contrastive learning strategy applied, our method further improves the DSC by 1.0%, 0.3% and 8.4% on GM, WM and CSF, respectively, over the V-Net variant. Notably, the improvement on CSF is much larger than that of GM and WM because GM and WM are majority classes and can be segmented satisfactorily. However, accurate CSF segmentation is the key to ensure topological correctness in reconstructing the pial surface.

Single modality We studied the performance of the proposed method with only either T1- or T2-weighted image as the input. The experimental results are shown in Table 2. Compared with the performance with paired T1- and T2-weighted images as input, the segmentation performance decreases marginally (ranging from -1.9% to -0.4% DSC). T1- and T2-weighted images provide complementary information that can help improve brain tissue segmentation. However, the marginal decrease indicates that our models learn effectively from limited information.

Growth modeling of tissue volumes We modeled the growth trajectories of predicted tissue volumes using generalized additive mixture model (GAMM). We fitted GAMM to the volume of each tissue type across the lifespan with cubic regression spline as smooth nonlinear function of age and subject-specific random intercept. The growth trajectories, shown in Fig. 2, indicate that the GM

and WM volumes exhibit an increase-then-decrease pattern; whereas the CSF volume increases throughout the lifespan.

Surface reconstruction Fig. 3 shows example white/pial surfaces and tissue segmentation maps generated using our method for various time points across the human lifespan. In general, the results indicate good segmentation details particularly at the cortex as evidenced by the detailed surface convolution with clear gyri and sulci.

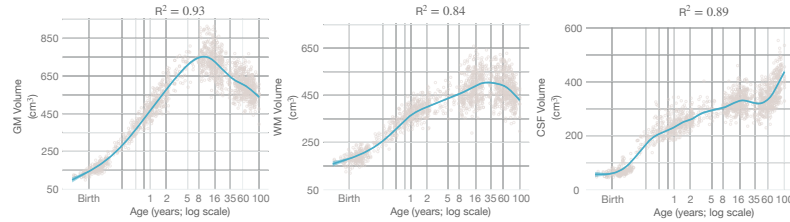


Fig. 2: Growth trajectories of tissue volumes across the human lifespan.

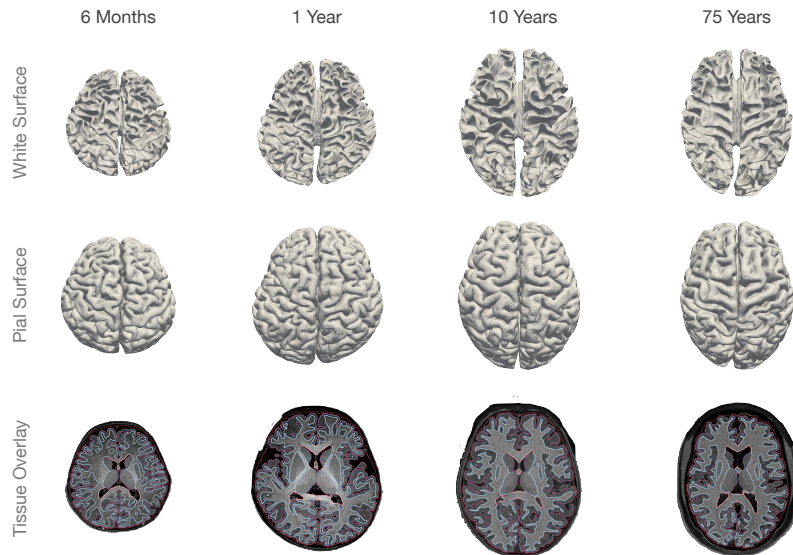


Fig. 3: Reconstructed white and pial surfaces and tissue segmentation maps at 4 different time points.

3.4 Ablation Study

Impact of using balanced losses We studied the impact of selecting equal number of voxels of different categories to compute both the CE and contrastive losses. As shown in Table 3, balancing the contributions from different class are critical to better segmentation of minority classes, e.g., the CSF.

Table 3: Impact of balanced losses on DSC.

	GM	WM	CSF
Unbalanced	93.6 ± 1.5	95.1 ± 1.3	83.0 ± 6.2
Balanced	94.2 ± 1.1	95.7 ± 1.0	88.5 ± 3.8

Impact of λ_{ctr} We fixed M to 10 and τ to 0.1. We tried 0.5 and 1.0 for λ_{ctr} . As shown in Table 4, the performance is marginally changed using different λ_{ctr} .

Table 4: Impact of λ_{ctr} on DSC.

	0.5			1.0		
	GM	WM	CSF	GM	WM	CSF
DSC	94.0 ± 5.1	95.5 ± 1.1	88.6 ± 3.6	94.2 ± 1.1	95.7 ± 1.0	88.5 ± 3.8

Impact of M and τ We fixed λ_{ctr} to 1 as it is found that the performance is insensitive to the choice of λ_{ctr} . As shown in Table 5, larger M and smaller τ seem generate better results. This is consistent with [2], where it is found that a larger number of negative samples is beneficial for contrastive learning.

Table 5: Impact of M and τ on DSC.

$\tau \setminus M$	5			10		
0.1	93.9 ± 5.2	95.5 ± 1.2	88.4 ± 4.0	94.2 ± 1.1	95.7 ± 1.0	88.5 ± 3.8
0.2	93.6 ± 5.6	94.8 ± 1.6	88.1 ± 4.2	93.9 ± 5.4	95.3 ± 1.3	88.2 ± 3.8

4 Conclusion

We have presented a novel supervised contrastive learning method for brain tissue segmentation across the human lifespan. Experimental results on a large dataset show that our method can effectively segment the tissues with paired T1- and T2-weighted images or with just T1- or T2-weighted images.

Acknowledgement

This work was supported in part by the United States National Institutes of Health (NIH) under grants EB008374 and MH125479. Data were provided in part by the developing Human Connectome Project, KCL-Imperial-Oxford Consortium funded by the European Research Council under the European Union Seventh Framework Programme (FP/2007-2013) / ERC Grant Agreement no. 319456. Data were provided in part by the Human Connectome Project, WU-Minn Consortium (Principal Investigators: David Van Essen and Kamil Ugurbil; 1U54MH091657) funded by the 16 NIH Institutes and Centers that support the NIH Blueprint for Neuroscience Research and by the McDonnell Center for Systems Neuroscience at Washington University.

References

1. Ashburner, J., Friston, K.J.: Unified segmentation. *NeuroImage* **26**(3), 839–851 (2005)
2. Chen, T., Kornblith, S., Norouzi, M., Hinton, G.: A simple framework for contrastive learning of visual representations. In: International conference on machine learning. pp. 1597–1607. PMLR (2020)
3. Fischl, B., Salat, D.H., Busa, E., Albert, M., Dieterich, M., Haselgrove, C., Van Der Kouwe, A., Killiany, R., Kennedy, D., Klaveness, S., et al.: Whole brain segmentation: automated labeling of neuroanatomical structures in the human brain. *Neuron* **33**(3), 341–355 (2002)
4. Glasser, M.F., Sotiropoulos, S.N., Wilson, J.A., Coalson, T.S., Fischl, B., Andersson, J.L., Xu, J., Jbabdi, S., Webster, M., Polimeni, J.R., et al.: The minimal preprocessing pipelines for the Human Connectome Project. *NeuroImage* **80**, 105–124 (2013)
5. He, K., Fan, H., Wu, Y., Xie, S., Girshick, R.: Momentum contrast for unsupervised visual representation learning. In: Proceedings of the IEEE/CVF Conference on Computer Vision and Pattern Recognition. pp. 9729–9738 (2020)
6. Howell, B.R., Styner, M.A., Gao, W., Yap, P.T., Wang, L., Baluyot, K., Yacoub, E., Chen, G., Potts, T., Salzwedel, A., et al.: The UNC/UMN Baby Connectome Project (BCP): An overview of the study design and protocol development. *NeuroImage* **185**, 891–905 (2019)
7. Makropoulos, A., Robinson, E.C., Schuh, A., Wright, R., Fitzgibbon, S., Bozek, J., Counsell, S.J., Steinweg, J., Vecchiato, K., Passerat-Palmbach, J., et al.: The developing human connectome project: A minimal processing pipeline for neonatal cortical surface reconstruction. *NeuroImage* **173**, 88–112 (2018)
8. Milletari, F., Navab, N., Ahmadi, S.A.: V-net: Fully convolutional neural networks for volumetric medical image segmentation. In: International Conference on 3D Vision (3DV). pp. 565–571. IEEE (2016)
9. Nie, D., Wang, L., Gao, Y., Shen, D.: Fully convolutional networks for multi-modality isointense infant brain image segmentation. In: IEEE International Symposium on Biomedical Imaging (ISBI). pp. 1342–1345 (2016)
10. Roy, A.G., Conjeti, S., Navab, N., Wachinger, C.: QuickNAT: A fully convolutional network for quick and accurate segmentation of neuroanatomy. *NeuroImage* **186**, 713–727 (2019)

11. Ulyanov, D., Vedaldi, A., Lempitsky, V.: Instance normalization: The missing ingredient for fast stylization. arXiv preprint arXiv:1607.08022 (2016)
12. Van Essen, D., Ugurbil, K., Auerbach, E., Barch, D., Behrens, T., Bucholz, R., Chang, A., Chen, L., Corbetta, M., Curtiss, S., Della Penna, S., Feinberg, D., Glasser, M., Harel, N., Heath, A., Larson-Prior, L., Marcus, D., Michalareas, G., Moeller, S., Oostenveld, R., Petersen, S., Prior, F., Schlaggar, B., Smith, S., Snyder, A., Xu, J., Yacoub, E.: The Human Connectome Project: A data acquisition perspective. *NeuroImage* **62**(4), 2222 – 2231 (2012)
13. Wen, Y., Zhang, K., Li, Z., Qiao, Y.: A discriminative feature learning approach for deep face recognition. In: European Conference on Computer Vision. pp. 499–515. Springer (2016)
14. Zhang, Y., Brady, M., Smith, S.: Segmentation of brain mr images through a hidden markov random field model and the expectation-maximization algorithm. *IEEE Transactions on Medical Imaging* **20**(1), 45–57 (2001)
15. Zöllei, L., Iglesias, J.E., Ou, Y., Grant, P.E., Fischl, B.: Infant FreeSurfer: An automated segmentation and surface extraction pipeline for T1-weighted neuroimaging data of infants 0–2 years. *NeuroImage* **218**, 116946 (2020)